

## Visualization of Submerged Cavitating Jet: Part Two – Influences of Hydrodynamic Conditions, Nozzle Geometry and Visualization System Arrangement

E.A. Hutli<sup>1</sup> (MSc), M. Nedeljkovic<sup>2</sup> (Professor) and Vojislav Ilic<sup>3</sup> (PhD)

<sup>1,2</sup> Department of Hydraulic Machinery and Energy Systems  
 Belgrade University, Faculty of Mechanical Engineering, Belgrade, Serbia

<sup>3</sup> School of Engineering, University of Western Sydney, Australia

### Abstract

In visualization results of highly-submerged cavitating water jet obtained by a digital camera, the influence of parameters such as: injection pressure, nozzle diameter and geometry, nozzle mounting (for convergent / divergent flow), cavitation number and exit jet velocity, were investigated. In addition, the influence of visualization system position was studied. All the parameters have been found to be of strong influence on the jet appearance and performance.

### Introduction

Flow visualization has been an important tool in fluid dynamics research; it has been used extensively in engineering, physics, medical science, meteorology, oceanography and aerodynamics etc. As can be determined from the published literature, not much is known about the unsteady behaviours of the cavitating jet and the development as well as the collapse of the cavitation clouds on the impinging surface. If the unsteady behaviour and the jet structure are clarified in detail, it is expected that, the jet working capacity can be drastically improved [2, 8]. The flow visualization is used here to achieve these goals. In this paper, NIKON COOLPIX 990 digital camera was used for visualization and investigation of the influences of hydrodynamic conditions, nozzle geometry, and position of the visualization system. The nozzles used are mounted to be suddenly convergent or divergent. The visualization investigations were done using a stroboscope for time 30  $\mu$ s to illuminate the cavitating jet. The flash frequency was 50 Hz while the shutter camera frequency was 1/30 or 1/60 s<sup>-1</sup>. The jet images were taken as a movie at around 600 frames in 40s (15 frames/s). The jet behaviour has then been followed by extracting appropriate images.

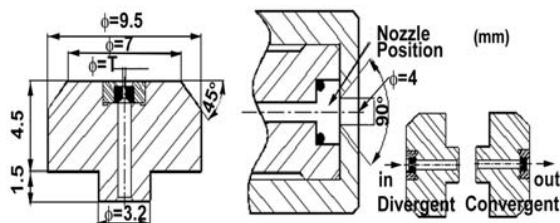


Figure 1. Nozzle geometry, nozzle holder, and the manner of nozzle mounting

### Influence of Nozzle Conicity

Investigation of the influence of nozzle conicity was done by mounting the nozzle in two ways, once to have a nozzle as suddenly divergent and once to have it suddenly convergent (Fig.1). The cavitation number was calculated as  $(\sigma = (P_2 - P_v) / (0.5\rho V_j^2))$ . The installation of the visualization system is shown in Fig.2 (left).

### Analysis for the Divergent Conical Nozzle

Divergent Nozzle, with inlet diameter of  $D_{in}=0.45$  mm and outlet of  $D_{out}=1$  mm, (divergent)

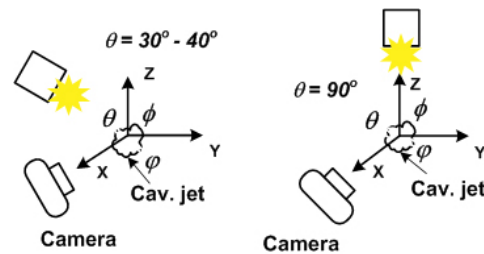


Figure 2. Arrangement of the apparatus.

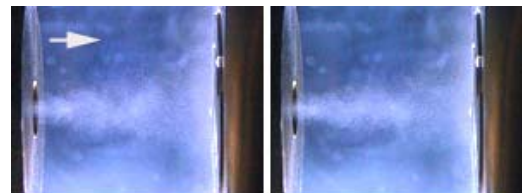


Figure 3. Appearance of the cavitating jet. Conditions:  $P_1=8$ bar,  $P_2=2.05$  bar,  $\sigma=17.85$ ,  $V_j=4.9$ m/s,  $T=16^\circ$ C, Divergent Nozzle.

In Fig.3 two images reveal that the jet is comprised only of very tiny individual bubbles (no clouds), the spreading angle of jet is bigger than the corresponding one in other images on the next figures for the same case. The existence of tiny bubbles is attributed to the inception of cavitation inside the nozzle (not at the nozzle outlet). Images in Fig. 4 show that the cavitation started to go out from the nozzle as dense clouds and then immediately transformed to lighter clouds, which appear as smoky clouds after a maximum distance of 20% of the distance between the nozzle exit and the target surface (which is denoted by X,  $X=25.67$ mm) (first 6 images). The analyses of the remaining groups of images in Fig.4 show that the jet penetration, jet breaking point position, jet-spreading angle, and jet density (individual bubbles and bubble clusters) are increased as upstream pressure ( $P_1$ ) increases. At the end of the jet, when the jet strikes the target wall at high  $P_1$ , it spreads radially and covers all the area with tiny bubbles. These bubbles collapse at different radial positions on the target surface or near it. The position of bubble collapse depends on the radial pressure distribution while the local stress produced as a result is a function of two parameters: the bubble content, and the bubble size.

### Analysis for the Convergent Nozzle

Figs.5, for convergent nozzle ( $D_{in}=1$  mm and outlet of  $D_{out}=0.45$  mm), reveals that the jet behaviour with up-stream pressure is the

same as in the case of Divergent Nozzle. However, the position of the breaking point, jet penetration spreading angle and the jet density in case of nozzle convergence are much bigger than for the divergent case. This is attributed to the big difference in the velocities for the two nozzle directions. In the case of convergent nozzle at  $P_1 = 8$  bar, no cavitation was observed. However, at  $P_1=25$  bar the phenomenon appeared at nozzle exit with irregular and rare frequency: it was unstable, and this can be assumed as the inception of cavitation (no image was obtained for this case). In the groups of images for  $P_1=145$  and  $195$  bar (Fig.5) many bubbles distributed throughout the whole area may be observed. This feature is related to the intensive vortex action in the jet, which leads to the liberation of bubble growth and their spreading and floating in the chamber. Finally, these bubbles collapse when they meet the point of sufficient pressure in their path. However, these gas bubbles have longer lifetime as compared to cavitation (vapour) bubbles.

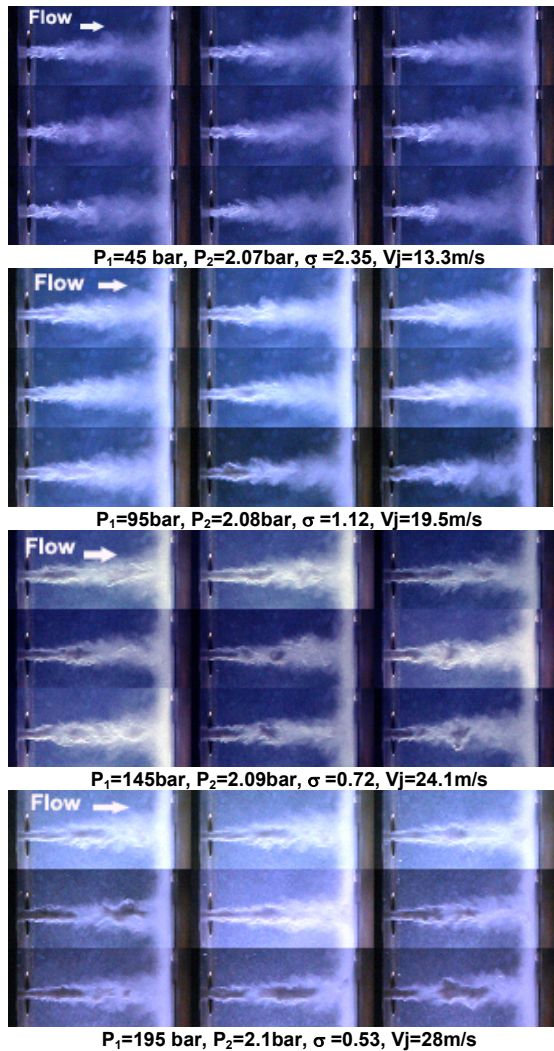


Figure 4. Cavitating jet started outside at the nozzle exit (divergent nozzle  $d_{in}=45mm$ ,  $d_{out}=1mm$ ),  $T=16^{\circ}C$ <sup>1</sup>

<sup>1</sup> NOTE: The given exit velocities ( $V_j$ ) during cavitation are based on the single phase flow. For the same mass flow rate, the actual flow velocity will be higher than given.

### The Influence of Nozzle Dimensions on the Cavitating Jet Behaviour

Visualizations of jets created by two different nozzles (both are Divergent Nozzles but of different dimensions) were done. Figures 6 and 7 represent the results. Upstream pressure ( $P_1$ ) was kept constant, as well as working fluid temperature and standoff distance, while jet velocity ( $V_j$ ) and downstream pressure ( $P_2$ ) changed with the nozzle geometry (thus the cavitation number also changed). The comparison of obtained results reveals that the cavitating jet characteristics are strongly dependent on geometry and diameter of the nozzle - jet penetration, jet width, jet spreading angle and cavitation cloud density are the parameters that significantly change with the nozzle geometry change.

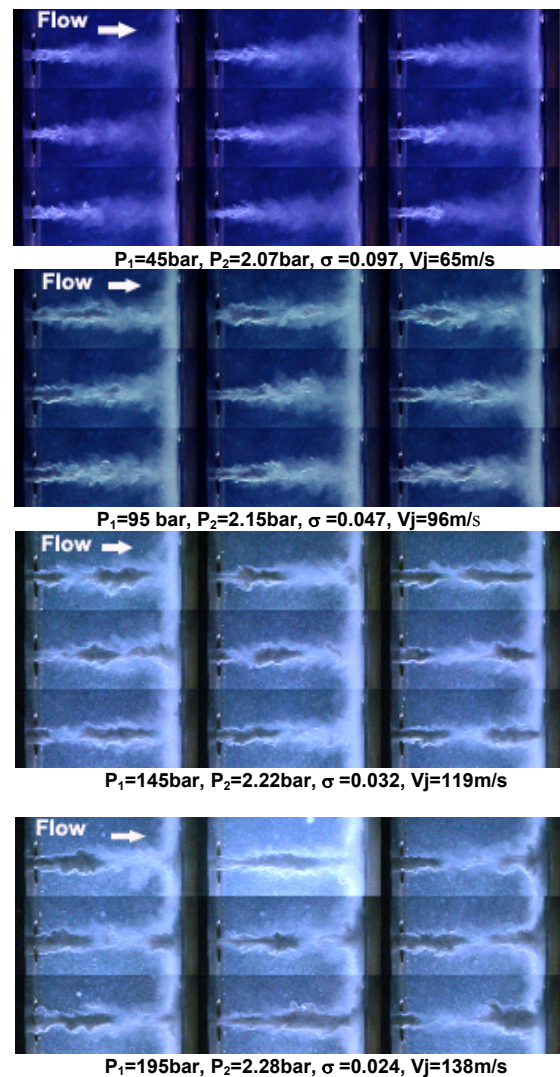


Figure 5. Cavitating jet started outside at the nozzle exit (Convergent nozzle  $d_{in}=1mm$ ,  $d_{out}=0.45mm$ ),  $T=16^{\circ}C$

They decreased as the inlet nozzle diameter decreased. Both gaseous and vaporous types of cavitation were observed in the present study. Gaseous type of cavitation occurred when the dissolved gases in high-pressure came out of solution with liquid in the low-pressure test section (test chamber), while vapor type cavitation, for a given liquid temperature, occurred when

reduction of pressure due to dynamic effects decreased to saturation pressure for that temperature, giving rise to evaporation (local boiling/cavitation). These two types of cavitation were quite distinct in appearance. The gaseous type seemed to be formed within the entire jet with bubbles of nearly spherical shape. Bubbles did not form clusters.

This type of cavitation is mainly dependent on upstream pressure  $P_1$ . The vapor type cavities strongly depend on the cavitation number. Relatively large coalescing vapor cavities may form away from, nearby or possibly inside the nozzle itself. Another interesting difference between the two types of cavitation is that the vapor cavities disappear after a certain distance from the nozzle, while the gaseous bubbles tend to persist indefinitely (only an increase of  $P_2$  destroys them). Gaseous cavities do not contribute to the erosion of material [6].

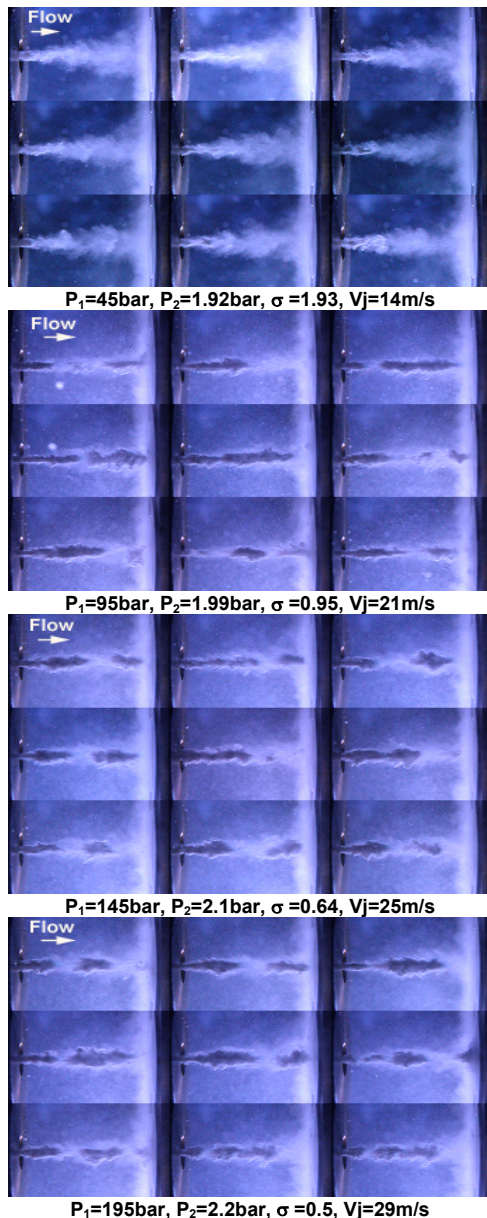


Figure 6. Cavitating jet started outside at the nozzle (Divergent nozzle  $d_{in}=0.55\text{mm}, d_{out}=1.1\text{mm}$ ),  $T=16^\circ\text{C}$

The formation of gaseous cavities in the present experiments could be suppressed by slight pressurization of the test section, since it was not possible to control the dissolved gases with degassing of water in the test rig system (the water is assumed to be saturated). The existence of these two types of cavitation at high upstream pressures (high vortices) may be clearly distinguished in the group of images in Figures 9-11 in the next paragraph (effect of cavitation, velocity and system arrangement) the gas bubbles appears as spots distributed randomly in the test chamber.

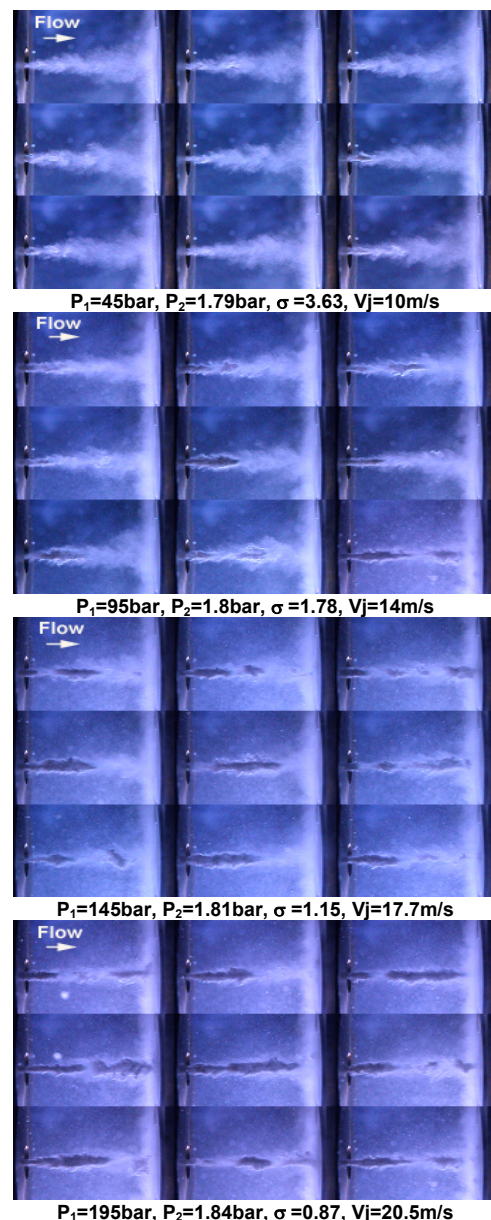


Figure 7. Cavitating jet started outside at the nozzle exit (Divergent nozzle  $d_{in}=0.4\text{mm}, d_{out}=1\text{mm}$ ),  $T=16^\circ\text{C}$

#### Influence of Cavitation Number ( $\sigma$ ) and Exit Jet Velocity ( $V_j$ ) on Characteristics of Cavitating Jets

In order to get better distribution of light to improve the quality of images, the flashlight and the camera eye were installed on the same side (same window). Since the window area is not large

enough to accept the camera and the flash together in parallel, the flash had to be inclined to the camera direction with an included angle  $\theta$  (between  $30^\circ$  and  $40^\circ$ ). The experimental installation is shown in Fig.2 (left). Visualizations were done using convergent nozzle ( $d_{in}=1m$  and  $d_{out}=0.45mm$ ) first for different cavitation numbers  $\sigma$ , which was achieved by changing the downstream pressure ( $P_2$ ) and second for different exit jet velocity ( $V_j$ ) which was achieved by changing upstream pressure ( $P_1$ ). Figs. 8 and 9 show the results, respectively. The visual analysis reveals that the jet appears as a complete solid unit in white colour.. The jet penetration is increased as  $\sigma$  or  $P_2$  is decreased and when jet strikes the target it starts spreading over the target surface and formation of rings appears. In the first row in Fig.9 the jet did not arrive to the target wall – it disappeared in the region of the second third of the full distance between the nozzle exit and the target wall (2/3 of X). The jet is more stable as  $V_j$  or  $P_1$  increase. Jet width and jet penetration increased as  $V_j$  or  $P_1$  increase.

These results are in good agreement with Soyama [4,5]. In the 2<sup>nd</sup> and 3<sup>rd</sup> row of images in Fig.8 and 3<sup>rd</sup>, 4<sup>th</sup> and 5<sup>th</sup> row of images in Fig.9, the gaseous bubbles appear as fog distributed in the chamber.

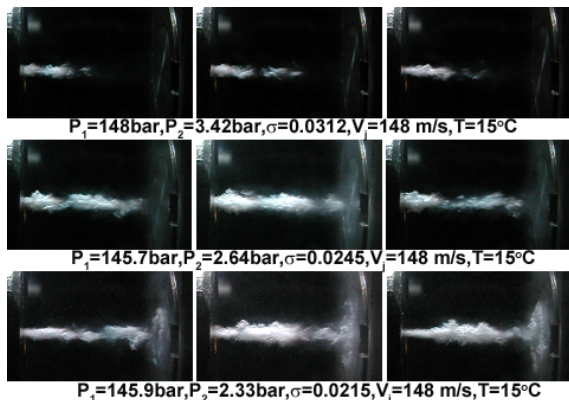


Figure 8. Influence of cavitation number on the jet behaviour.

### Influence of Visualization System Arrangement on the Information Content In Cavitating Jet Images

In the first case the visualization was made with a sheet of white paper between the flash and the window. The reason for this was to reduce the intensity of light illuminating the jet before entering the camera. In addition, the paper enhances the distribution of the light in the test chamber Fig.10 (right). In the second case, the visualization was made by mounting the flash in such a way to be in parallel with the jet direction (in the same direction of the flow, Fig.10 (Left (no paper))). The light was from the other side of the test chamber with the angle  $\varphi = 90^\circ$  to the camera eye i.e. the flash was at right angles to the camera. Fig.11, 12 and 13 shows the results (right column in each figure for 1<sup>st</sup> case while Left column for 2<sup>nd</sup> case). The comparison between the two cases reveals that, the position of light and its distribution is very important factor in the information provided by the visualization process for the cavitating jets. In first case the cavitating jet appears as a dark grey shadow. It seems less dense and is discontinuous in some locations.

The difference in the jet features compared with the second case may be attributed to the light passing through the jet here, such that the jet appears discontinuous.. Also, there exists a reflection process of light by the spherical bubbles in or around the jet. However, this reflection is not in the direction of the camera eye,

so the camera does not sense the reflected light. All these factors, including the limitation of camera resolution, contribute to the fact that bubbles will not appear in the images and the jet appears as a dark grey shadow.

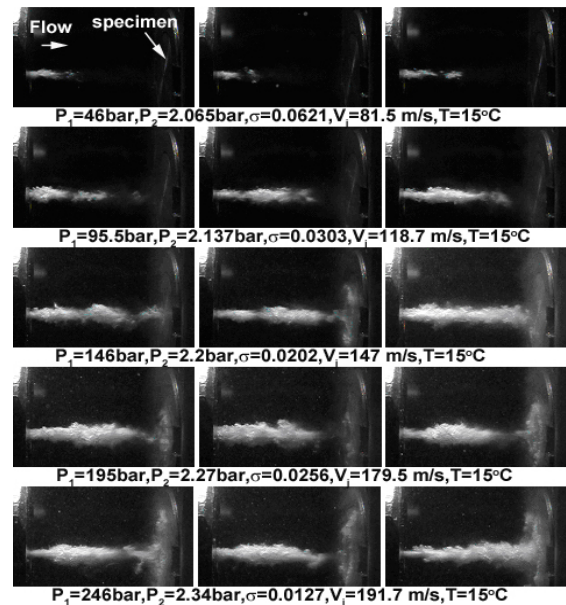


Figure 9. Influence of exit jet velocity ( $V_j$ ) on the jet behaviour.

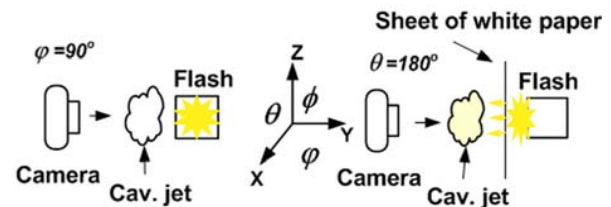


Figure 10. Visualization system

In the second case, and in the two cases when flash was mounted as in Fig.2 (both left and right), the light was reflected by the spherical bubbles, thus the distances between the cavitation clouds (or clusters of bubbles), as a result of the break off, were allowed to be seen. The rest of the jet appears as a white portion and it contains many tiny bubbles that may reflect some light to the direction of the camera. In Fig.10 at  $P_1=145$  bar, the gas bubbles appear in the images for the second case. However, this was not observed in the first case. At  $P_1=195$  bar, the gas bubbles appear in both cases, which may be explained by the appearance of greater number of bubbles at pressure  $P_1=195$  bar than at  $P_1=145$  bar. However, the bubble density (number of bubbles) which appears in the images obtained in first case is much less than that which appears in the images obtained by the second case. Thus we can notice how the information in the image depends on the arrangement of the visualization system.

The interesting point worth mentioning in the end is that the definition of cavitation number ( $\sigma = P_2/P_1$  as proposed by ASTM ) is not enough to describe the phenomenon or is incorrect since the geometry is not included. The normal definition ( $\sigma = (P_2 - P_v)/(0.5\rho V_j^2)$ ) is more convenient way to describe the phenomenon, even if it is not descriptive enough of the whole phenomenon. However this definition provides values of  $\sigma$  lower

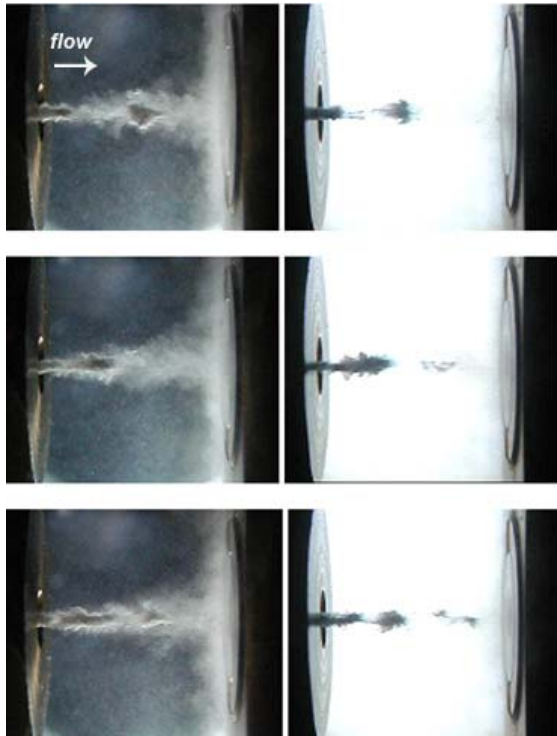


Figure 11. Influence of visualization system arrangement on the visualization data. ( $P_1=95\text{bar}$ ,  $P_2=2.08\text{bar}$ ,  $\sigma=1.12$ ,  $V_j=19.5\text{m/s}$ ,  $T=16^\circ\text{C}$ )

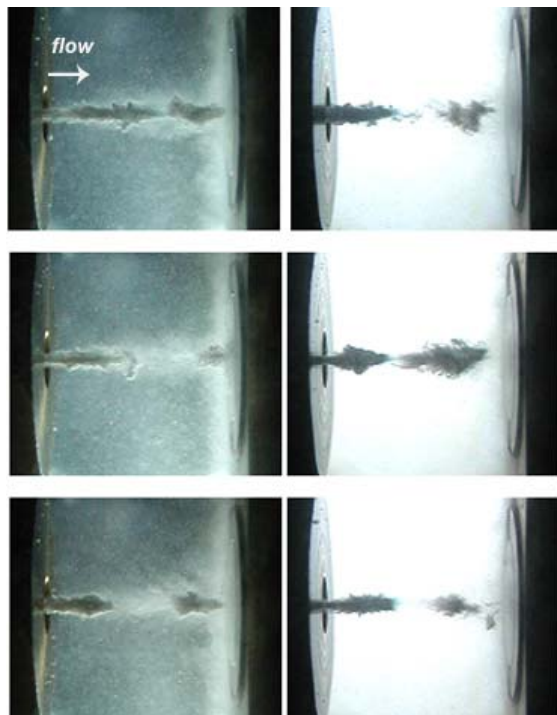


Figure 12. Influence of visualization system arrangement on the visualization data. ( $P_1=145\text{bar}$ ,  $P_2=2.09\text{bar}$ ,  $\sigma=0.72$ ,  $V_j=24.1\text{m/s}$ ,  $T=16^\circ\text{C}$ )

when cavitation is more intense, which appears reasonable. This may be seen by comparing Figures 4-7.

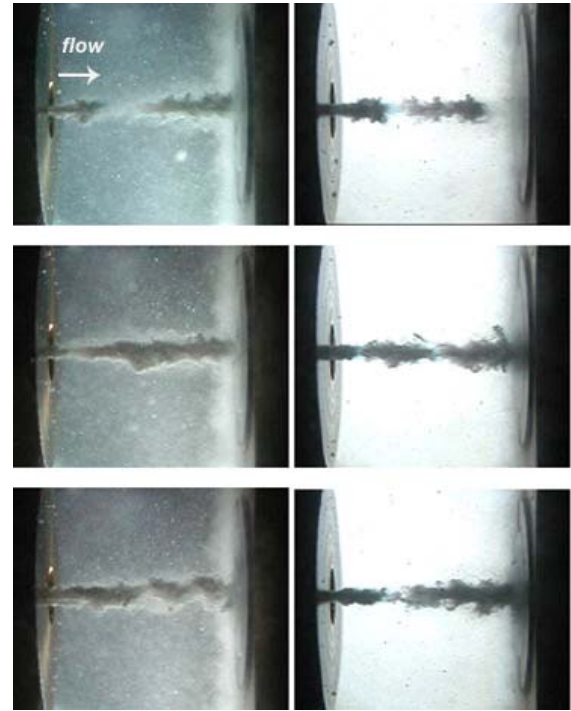


Figure 13. Influence of visualization system arrangement on the visualization data. ( $P_1=195\text{bar}$ ,  $P_2=2.1\text{bar}$ ,  $\sigma=0.53$ ,  $V_j=28\text{m/s}$ ,  $T=16^\circ\text{C}$ )

### Conclusion

The jet behaviour and its features depend on nozzle mounting (convergent or divergent configuration). The hydrodynamic conditions for cavitation inception and its position depend on the nozzle geometry. The hydrodynamic condition has a big influence on the jet behaviour and its features. Both gaseous and vapor types of cavitation appear at high upstream pressures. The life of gaseous cavitation is longer than of vapour cavitation. Vapor types of cavitation depend on cavitation number or on downstream pressure  $P_2$ , while gaseous cavitation depends mainly on upstream pressure  $P_1$ . Both of them depend on the nozzle geometry. The visualization arrangement has a big influence on the quality of jet images, and hence on the information that can be obtained from them. The difficulties of capturing the instant of the collapsing bubbles are related to inadequate temporal resolution of illuminating and recording system, and the huge number of the bubbles in the cavitating jet.

### Nomenclature

$\sigma$  cavitation number

$$\sigma = \frac{P_{ref} - P_v}{\frac{1}{2} \rho u_{ref}^2}$$

$P_{ref}$  Reference (downstream) pressure (bar)

$P_v(T)$  Saturation (vapor) pressure (bar),

$\rho_L(T)$  Density of the liquid ( $\text{kg/m}^3$ ),

$T$  Fluid temperature [ $^\circ\text{C}$ ]

$u_{ref}$	Reference velocity - exit jet velocity (m/s) = $Q / A = V_J$
Q	= $K * \sqrt{(P_1 - P_2)}$ - flow rate (m <sup>3</sup> /s)
A	Nozzle outlet cross-section area (m <sup>2</sup> )
P <sub>1</sub>	Upstream pressure (bar) (absolute)
P <sub>2</sub>	Downstream pressure (bar) (absolute)
X	Stand-off distance (mm)
L	Nozzle length
d <sub>in</sub> , d <sub>uot</sub>	Inlet and outlet nozzle diameter (mm)
K	= 4.78E-09 for divergent ; = 6.17E-09 for convergent nozzle (m <sup>3</sup> /s/Pa <sup>1/2</sup> )

### References

- [1] Keiichi S, Yasuhiro S. Unstable Cavitation Behaviour in a Circular-Cylindrical Orifice Flow. Trans JSME, International Journal, Ser.B, Vol.45, No.3, pp.638-645, 2002
- [2] Ganippa LC, Bark G, Andersson S, Chomiak J. Comparison of Cavitation Phenomena In Transparent Scaled-Up Single-Hole Diesel Nozzles, CAV2001, session A9.005, 2001.
- [3] Soyama H., High-Speed Observation of a Cavitating Jet in Air. Trans ASME, Journal of Fluids Engineering, Vol. 127, pp 1095-1101, November 2005.
- [4] Soyama H, Ikohagi T, Oba R. Observation of the Cavitating Jet in a Narrow Watercourse, Cavitation and Multiphase Flow, ASME, FED-Vol.194, 79-82, 1994.
- [5] Soyama H, Lichtarowicz A, Lampard D. Useful Correlations for Cavitating Jets, 3<sup>rd</sup> international symposium on cavitation, Grenoble, France, 1998.
- [6] Vijay MM, Zou C, Tavoularis S. A Study of the Characteristics of Cavitating Water Jets by Photography and Erosion Jet Cutting Technology – Proceedings of 10<sup>th</sup> International Conference, 37-67, Elsevier 1991.